



**HAL**  
open science

## Scheimpflug Self-Calibration Based on Tangency Points

Thierry Fournel, Hanene Louhichi, Cécile Barat, Jean-François Menudet

► **To cite this version:**

Thierry Fournel, Hanene Louhichi, Cécile Barat, Jean-François Menudet. Scheimpflug Self-Calibration Based on Tangency Points. The 12th International Symposium on Flow Visualization, Sep 2006, Göttingen, Germany. ujm-00378467

**HAL Id: ujm-00378467**

**<https://ujm.hal.science/ujm-00378467>**

Submitted on 24 Apr 2009

**HAL** is a multi-disciplinary open access archive for the deposit and dissemination of scientific research documents, whether they are published or not. The documents may come from teaching and research institutions in France or abroad, or from public or private research centers.

L'archive ouverte pluridisciplinaire **HAL**, est destinée au dépôt et à la diffusion de documents scientifiques de niveau recherche, publiés ou non, émanant des établissements d'enseignement et de recherche français ou étrangers, des laboratoires publics ou privés.

# SCHEIMPFLUG SELF-CALIBRATION BASED ON TANGENCY POINTS

T. Fournel<sup>1</sup>, H. Louhichi<sup>1,2</sup>, C. Barat<sup>1</sup>, J.F. Menudet<sup>1</sup>

<sup>1</sup>Laboratoire Traitement du Signal et Instrumentation, UMR Université J.Monnet-CNRS 5516,  
18 rue Lauras 42000 Saint Etienne, France

<sup>2</sup> Unité de Métrologie en Mécanique des Fluides et Thermiques, UR 11-17, rue Iben Eljazzar,  
5019 Monastir, Tunisie

**Keywords:** *Tangency points, Self-calibration, Scheimpflug model*

## ABSTRACT

*The performance of camera self-calibration is strongly dependent on the accuracy of the detection of feature points in images. This paper highlights the bias introduced in the estimate of Scheimpflug camera parameters when using dot centres as feature points. This offset due the perspective projection causes major errors when using too large dots. A generic approach, suited to any setting, which takes advantage of the invariance property of tangency points under perspective projection is introduced. New feature points are introduced and their robust extraction proposed. The resulting method leads to a simple and efficient calibration pattern. Experimental results on both simulated and real data show the relevance of the proposed method.*

## 1 INTRODUCTION

The Scheimpflug condition is used in Stereoscopic Particle Image Velocimetry (SPIV) for measuring velocity fields with an angular set-up [1][2]. A traditional approach for the preliminary step of the camera calibration is to image a target after some known displacements and to deduce the mapping functions from feature correspondences [3]. For reliable results, this approach requires an accurate positioning of a high-precision target in space. In order to relax these practical constraints which are respectively time-consuming (especially in large test facilities) and costly (one high-precision target per magnification range), self-calibration of Scheimpflug cameras was proposed [4]. A bundle adjustment technique which is a non-linear least square optimization method, allows the estimate of both the camera parameters and the coordinates of the control points. However the performance of such a calibration is strongly dependent on the accuracy of the detection of feature points in images [5]. (Commercial) targets of circular dots are frequently used for calibrating SPIV systems. The centres of the dots classically serve as feature points.

Given a dot, an offset exists between the detected centre of the image dot and the perspective projection of the dot centre considered as feature point [6]. This offset is increased when tilting the sensor in order to perform the Scheimpflug condition. Ignoring this offset may appear in contradiction with

the considerable attention paid to sub-pixel detection of dot centres and can induce error propagation in calibration. In order to overcome this problem without marking dots, one approach consists in the introduction of a bias correction in the camera model [7]. In this paper we introduce a more generic approach, suited to any setting, which takes advantage of the invariance property of tangency points under perspective projection: tangency points serve as control points and their projections are used for calibrating without any offset. These points are defined by common tangents to pairs of dots (circles or ellipses). The method proposed for the image detection of tangency points has five steps: a local scale-adaptive edge detection, a labelization of image dots, a least square fit of image dot edges and the computation of common tangents and tangency points. Because of the stability of the ellipse fitting algorithm [9], high accuracy on these features can be expected.

Self-calibration by bundle adjustment is described together with the camera model in section 2. In section 3 an expression for the offset in Scheimpflug condition is derived and its influence discussed. Section 4 is dedicated to the proposed approach based on tangency points as control points. Finally, experimental results are reported in section 5. The influence of the edge detection error in the computation of tangency points is studied on simulated data then the solution is applied in real conditions.

## **2 BUNDLE ADJUSTMENT FOR SCHEIMPFLUG SELF-CALIBRATION**

The self-calibration of a video-camera aims to extract the intrinsic parameters of the camera from a sequence of views of the scene. When the scene is natural, it is classically performed by considering some properties of projective geometry and an adequate camera motion [10]. In some metrological applications, one can rather prefer to introduce a calibration pattern which can be optimized together with the camera parameters by bundle adjustment [5]. This last technique is a least mean square method which can be extended to Scheimpflug configuration by modifying accordingly the camera model [4]. By recording a set of views of the target, such an adjustment allows a reliable estimation of the parameters because high redundancy is obtained by separating extrinsic from intrinsic parameters of the camera. Thus redundancy becomes high enough to self-calibrate i.e. to introduce the coordinates of the calibration points into vector  $\Phi$  of parameters to be adjusted by least mean squares. The achievement of such calibration is strongly dependent on the accuracy of the detection of some feature points in images. Usually, a precision of about 0.02 pixel is required [5].

### **2.1 Camera model**

The Scheimpflug camera model is derived from the pinhole one by tilting the sensor (or the lens) according to an angle  $\theta$ . The tilt is performed accordingly to the Scheimpflug condition. This condition satisfied when the image plane, the lens plane and the object plane intersect in a common line (Fig. 1), ensures that conjugaison formula  $\frac{1}{f} = \frac{1}{p_i} + \frac{1}{p_o}$  is verified. With nominal magnification  $M = \frac{p_i}{p_o}$  and view angle  $\alpha$ , tilt  $\theta$  is given by:

$$\theta = \arctan(M \tan(\alpha)) \tag{1}$$

Under the pinhole model the relation between a 3D point  $\mathbf{X} = (X, Y, Z, 1)^T$  in the world frame  $W$  and its image  $\mathbf{x}_p = (x, y, z, 1)^T$  in the camera frame  $C$  is described by the following expression:

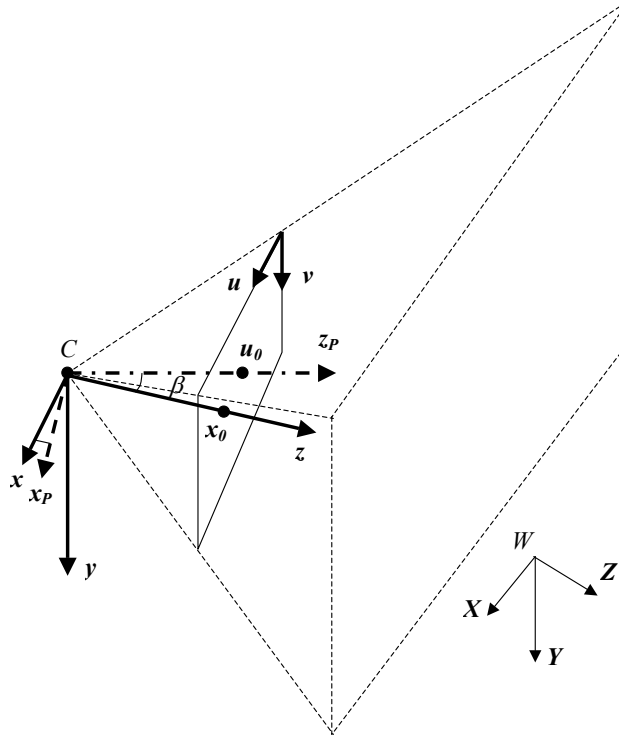


Fig. 1 Coordinate systems in Scheimpflug condition according to the "painter convention".

$$\mathbf{x}_P \approx \mathbf{P}_P \begin{bmatrix} \mathbf{R}_P & \mathbf{t}_P \\ \mathbf{0}^T & 1 \end{bmatrix} \mathbf{X} + \delta \mathbf{x} \quad (2)$$

where the equivalence relation denoted by symbol  $\approx$  means equality up to a non zero scale factor.  $\mathbf{R}_P$ ,  $\mathbf{t}_P$  are the rotation and translation matrices relating the world coordinate system to the camera one,  $\mathbf{P}_P$  is the perspective projection to the frontal plane and where  $\delta \mathbf{x}$  is the distortions term. The Scheimpflug

model induces tilt angle  $\theta$  of the image plane as supplementary parameter. Image  $\mathbf{x}$  can be deduced from  $\mathbf{x}_P$  by:

$$\mathbf{x} \approx \begin{bmatrix} \mathbf{R}_S & \mathbf{0} \\ \mathbf{0}^T & 1 \end{bmatrix} \mathbf{P}_S \mathbf{x}_P \quad (3)$$

where  $\mathbf{P}_S$  is the perspective projection in the image plane and  $\mathbf{R}_S$  is the (Scheimpflug) rotation of the camera coordinate system which leads the optical axis to merge in the normal of the tilted image plane.

## 2.2 Solution of the problem

Calibration points are estimated simultaneously with the camera parameters by minimizing image residual errors as:

$$\begin{cases} \varepsilon_U = u - \hat{u} \\ \varepsilon_V = v - \hat{v} \end{cases} \quad (4)$$

where  $(\hat{u}, \hat{v})$  are the pixel coordinates of the projection of a calibration point given by the camera model and  $(u, v)$  are the measured ones. The problem is to estimate the vector  $\Phi$  by minimizing the sum of the square residual errors:

$$S = \sum_{i=1}^n \sum_{j=1}^m (\varepsilon_{u_{i,j}}^2 + \varepsilon_{v_{i,j}}^2) \quad (5)$$

From image coordinates  $(u_{i,j}, v_{i,j})$  of  $n$  calibration points  $(X_i, Y_i, Z_i)$ , measured in  $m$  views. As residual errors are non-linear functions of  $\Phi$ , the minimization is a non-linear optimization problem. One way of solving the problem is to linearize (4) with some initial value  $\Phi^{(0)}$  and solve for  $\Delta\Phi$  then by adding  $\Delta\Phi$  to  $\Phi^{(0)}$  as the new initial value and repeating the process until a certain convergency is satisfied.

Vector  $\Phi$  to be estimate consists of the intrinsic, the extrinsic and the  $3n$  coordinates  $(X_i, Y_i, Z_i)$  of the  $n$  calibration points. the intrinsic parameters consist in tilt angle  $\theta$  and the pinhole parameters: image distances  $p_x, p_y$  expressed in pixel, pixel coordinates  $(u_0, v_0)$  of the image centre and distortion coefficients  $a_1, a_2, a_3$ .  $m$  different positions of the target gives  $6m$  extrinsic parameters: Euler angles  $\alpha^{(k)}, \beta^{(k)}, \gamma^{(k)}$  of rotation  $\mathbf{R}_P$  and components  $t_x^{(k)}, t_y^{(k)}, t_z^{(k)}$  of translation  $\mathbf{t}_P$ . The set of the parameters can now be listed as follows:

$$\Phi_{8+6m+3n} = (p_x, p_y, u_0, v_0, a_1, a_2, a_3, \theta, \alpha^{(1)}, \beta^{(1)}, \gamma^{(1)}, t_x^{(1)}, t_y^{(1)}, t_z^{(1)}, \dots, \alpha^{(m)}, \beta^{(m)}, \gamma^{(m)}, t_x^{(m)}, t_y^{(m)}, t_z^{(m)}, X^{(1)}, Y^{(1)}, Z^{(1)}, \dots, X^{(m)}, Y^{(m)}, Z^{(m)})^T$$

Redundancy  $\rho$  given by the difference between the number of equations (4) and the number of  $8 + 6m + 3n$  unknown parameters is equal to:

$$\rho = 2mn - (8 + 6m + 3n) \quad (6)$$

## 3 THE OFFSET PROBLEM

As a circular dot projects to an elliptical one under perspective projection, let us point out that its centre does not project to the geometric ellipse centre. This fact can cause a non negligible bias error when feature point detection in images consists in the detection of centres of image dots. The resulting offset between the detected centre and the actual projection remains negligible in most computer vision applications. However it can induce a major source of errors in angular SPIV as the working distance is

low and the sensor tilted in order to perform the Scheimpflug condition. Besides, a subpixel accuracy in feature point detection is generally required in order to recover calibration parameters by bundle adjustment: typically less than 0.02 pixel. In this section, an expression for the offset is derived and its influence is discussed.

### 3.1 Analytic expression for the offset

Let us assume that the camera is mounted according to the Scheimpflug condition and that a target of circular dots is pointed out under viewangle  $\alpha$  at working distance  $p_o$ . The diameter  $[BD]$  of a given circular dot in the object plane can be projected onto the image plane as  $[bd]$  (Fig. 2). Dot center  $C$  is projected onto the image plane as  $c$ . Point  $A$  is the intersection between the object and the image cross-lines. Offset  $e$  which corresponds to the distance between point  $c$  and the center of segment  $[bd]$  can be defined as:

$$e = \frac{1}{2}(bc - dc) \quad (7)$$

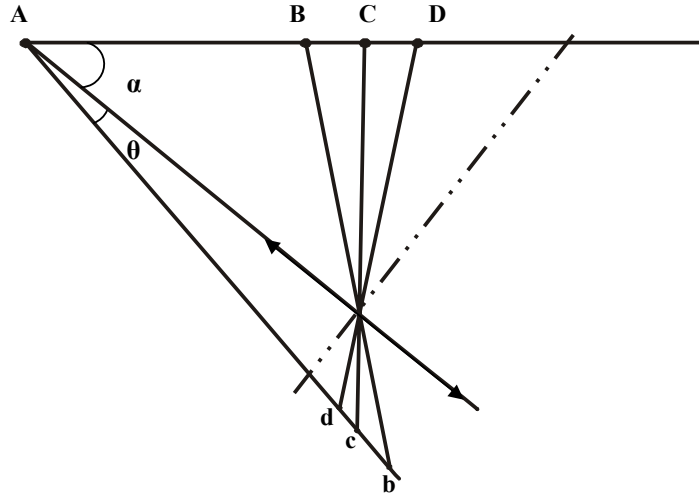


**Fig. 2** Offset in Scheimpflug configuration.

To establish its expression as a function of the model parameters, we based our calculations on the notion of cross-ratio of four collinear points. Let us consider the four points  $A$ ,  $B$ ,  $C$  and  $D$ . The cross-ratio is defined as:

$$\tau(A, B, C, D) = \frac{AB}{AC} \frac{BD}{AD} \quad (8)$$

Combining equations (7), (8) and the coordinates of points  $A$ ,  $B$ ,  $C$ ,  $D$  and the coordinates of their projections  $a$ ,  $b$ ,  $c$ ,  $d$  in the camera frame, offset  $e$  can be expressed in the pixel array as follows:

$$e = r \frac{R}{p_o} \frac{\sin(2\alpha)}{8 \cos(\theta)} \quad (9)$$

where  $R$  is the dot radius and  $r = M \cdot R / dx$  is the image dot radius expressed in pixel.

Thus, offset  $e$  is mainly function of working distance  $p_o$ , radii  $R$  in mm,  $r$  in pixel and view angle  $\alpha$  (Scheimpflug angle  $\theta$  given by (1) is usually about a few degrees).

### 3.2 Offset and recording conditions

Size  $r$  of the dot image at the centre of the field of view is often fixed in practice to a desirable value. Consequently offset  $e$  decreases linearly with  $R/p_0$  at a given view angle  $\alpha$ . Figure 3 shows offset  $e$  with respect to working distance  $p_0$  when viewing dots of radius 5 mm with  $r = 20$  pixel in image plane under  $\alpha = 45^\circ$ . The size of pixels was fixed to  $dx = 6.25\mu\text{m}$  with ratio  $dx/dy = 1$ . Until  $p_0 = 1.20$  m, the offset is superior to the precision required for image detection when self-calibrating (about 0.02 pixel). In this case, magnification is  $M = 0.05$ . The offset remains of the order of 0.01 pixel when increasing magnification  $M$  until 0.25 for  $r = 20$  pixel at  $p_0 = 500$  mm. To avoid the offset problem can be achieved by using small calibration dots. Dot radius  $R$  should be less than 1 mm in the range 0.05-0.5 of standard magnification in SPIV.

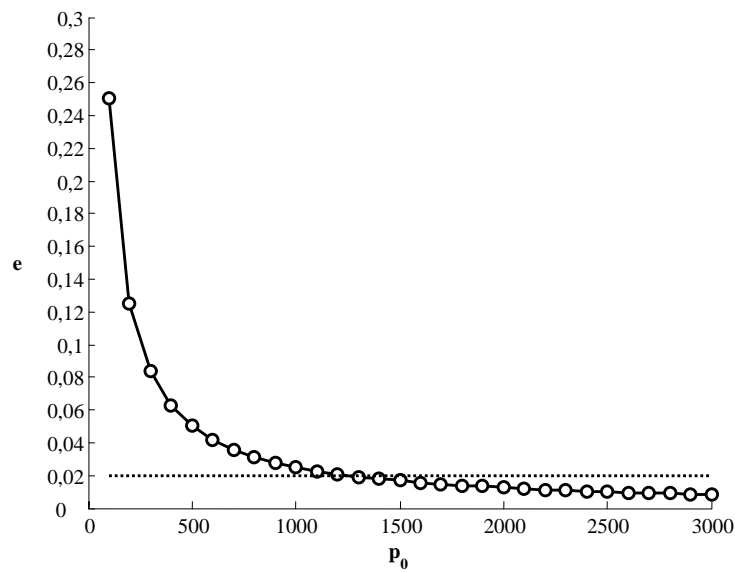


**Fig. 3** Offset  $e$  vs working distance  $p_0$  ( $M = 0.05$ ,  $R = 5$  mm,  $r=20$  pixel).

## 4 COMPUTING TANGENCY POINT COORDINATES

Another solution is to rather calibrate with larger dots by using some other feature points with a specific image detection. In this section we introduce new control points invariant under perspective projection. By exploiting the following property of Theory of perspective projection:

*The perspective projection of a tangent to a differentiable curve in 3D space at a point  $P$  of this curve is identical to the tangent to the projection of this curve at a point equal to the projection of  $P$ ,*

we propose to use points tangent to dots and their projections in images to perform calibration. The tangency points will be determined by selecting bi-tangents i.e. tangents common to a pair of dots. In the case of two separated ellipses, there exist four bi-tangents, two internal (LR, RL) and two external (LL,RR). In this way, 6 intersections between bi-tangents can be added as invariant points to the 8 tangency points as shown in figure (4) in order to get more feature points. For these points which does not require to mark dots, there is no offset due to the perspective projection.

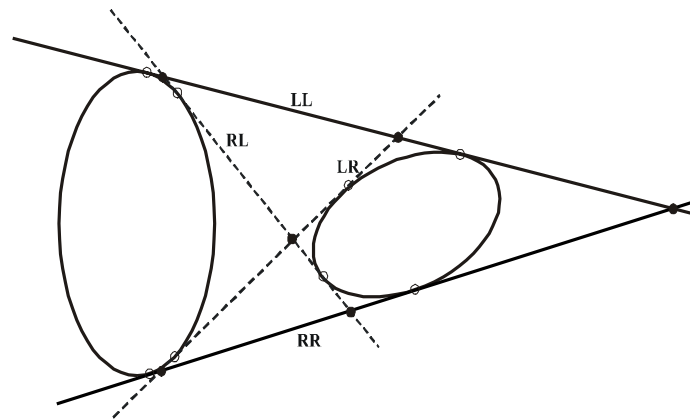


**Fig. 4** Bitangents and associated feature points.

For a given image of ellipses, the remaining question is how to compute the tangency points with subpixel accuracy, robustness to noise and efficiency.

Five steps are necessary to locate accurately the tangency points on images of ellipses:

- Ellipse edge detection
- Object labeling and ordering
- Ellipse model fitting
- Bitangent computation
- Feature point computation

The objective of the first three steps is to accurately estimate the parameters of the different ellipses and their relative positions with respect to a given pattern. The more robust the estimation, the more accurate the tangency points and consequently, the more reliable the calibration. As a consequence, it is essential to perform ellipse edge detection with great care using a robust method. Let us take a closer look at this first step. Since we work with oblique images, object circles are not perfectly focused and their images can even appear blurred. The amount of blur varies across the image plane in relation with the depths of the image points. Therefore, it is necessary to adopt a multi-scale edge detection method which adapts locally. The method described by Ducottet et al in [11] full fills these requirements. Indeed, it is a scale-adaptive method well suited to detect edges smoothed by Gaussian blur. It returns a set of connected edge pixels per ellipse. A standard object labelization is then applied in order to assign a number to each connected component. To put in correspondence the ellipses in images with their corresponding circles in space starts by identifying the ellipse at the upper-left corner and goes on by ordering ellipses from the reference one to determine the neighborhood relation between ellipses. The next step is to determine the five parameters describing each ellipse. A least square ellipse fitting is applied to each labeled object as proposed in [9]. It is a robust method which provides coordinates of ellipse centres and axes with subpixel accuracy. The two last steps correspond to the computation of the tangency points and of the intersections between bi-tangents.

## 5 EXPERIMENTAL RESULTS

### 5.1 Simulated data

In order to estimate the mean error and its standard deviation of the computed features in function of the noise level on the detected edge points in images, a setup of two ellipses was considered. Ellipses with semi-axes 100 and 200 pixel were oriented as shown in Fig. 4. With such a relative orientation, tangency points correspond to edge points where curvature is high. It will allow a more accurate detection. Results concerns 13 feature points: 8 tangency points and 5 intersections between bitangents (the point resulting from intersection of bitangents  $LL$  and  $RR$  is discarded because of its instability). The coordinates of 971 evenly spaced edge points were corrupted with a centered Gaussian distribution having standard deviation  $\sigma$ . Figures 5 and 6 show the mean error and the standard deviation respectively, estimated after 100 trials at different values of  $\sigma$ . The mean error remains inferior to 0.02 pixel for each feature point even for  $\sigma = 1$  pixel. However for such a subpixel accuracy, the standard deviation of error limits the acceptable level of noise to  $\sigma = 0.3$  pixel.

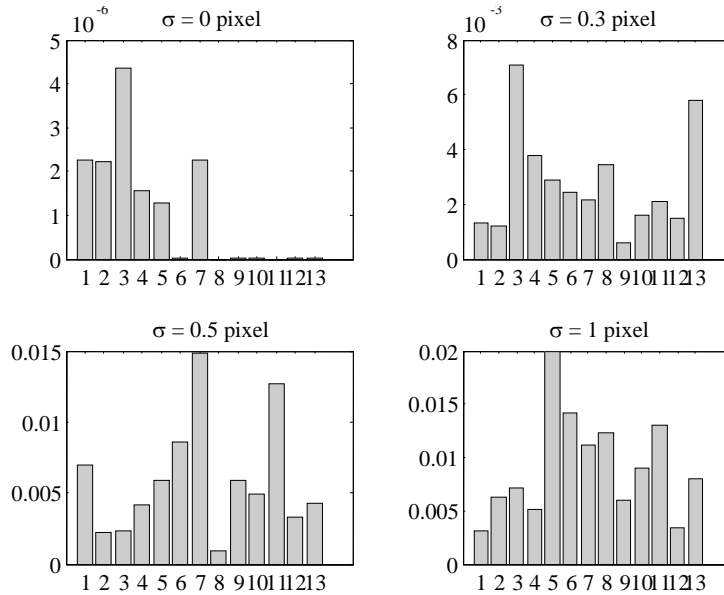
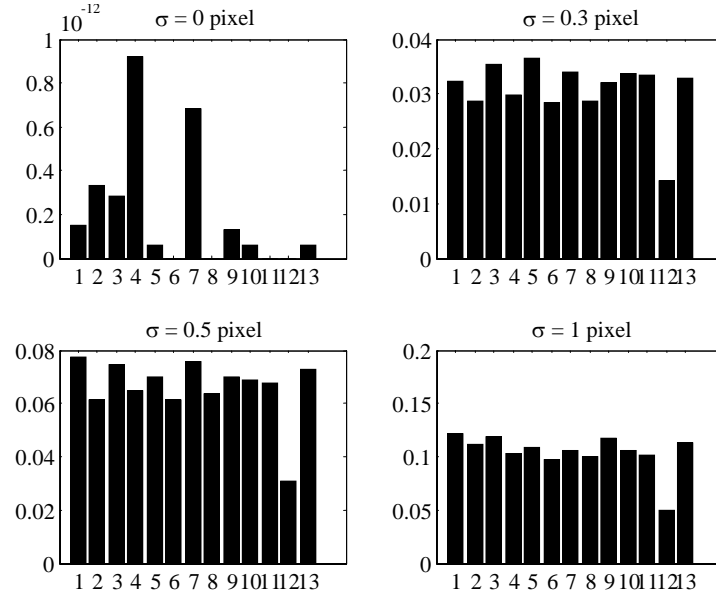


Fig. 5 Mean error for each of the 13 feature points.

### 5.2 Real data

Experiments in real conditions were performed at  $M = 0.05$  and  $f^\# = 1.8$  with a  $1/2''$  CCD camera having  $1024 \times 768$  pixel of size  $6.25\mu\text{m} \times 6.25\mu\text{m}$ . Camera was equipped with a  $f=50$  mm lens viewing under  $\alpha = 0^\circ$  then  $\alpha = 30^\circ$  by rotating the reference plane and  $\alpha = 45^\circ$  with Scheimpflug tilt. Two procedures were used for self-calibrating the camera. In the first procedure, the centres of  $5 \times 5$  dots of radius 5 mm located on a regular planar grid by step of 10 mm were detected with a specific algorithm based on the geometry and radiometry of dots [5]. In the second procedure, the points belonging to the bitangents of two ellipses oriented as shown in Fig. 4 having semi-axes 100 and 40 pixel, 90 and 45 pixel respectively,



**Fig. 6** Standard deviation for each of the 13 feature points.

Feature points	$\alpha(^{\circ})$	$p_x(\text{pixel})$	$p_y(\text{pixel})$	$u_0(\text{pixel})$	$v_0(\text{pixel})$	$a_1$	$a_2$	$a_3$	$\theta(^{\circ})$
Dots centres	0	$8000 \pm 0.67$	$8006 \pm 0.59$	$510 \pm 0.43$	$382 \pm 0.51$	$4.12 \pm 0.38$	$1.38 \pm 0.21$	$0.98 \pm 0.84$	-
	30	$6670 \pm 143.54$	$4393 \pm 67.39$	$605 \pm 23.67$	$448 \pm 106.87$	$10.26 \pm 5.43$	$-8.87 \pm -3.21$	$-30.63 \pm 12.31$	-
Tangency points	0	$8010 \pm 0.42$	$8009 \pm 0.36$	$510 \pm 0.65$	$379 \pm 0.37$	$3.89 \pm 0.21$	$1.08 \pm 0.54$	$0.82 \pm 0.11$	-
	30	$8012 \pm 0.31$	$8014 \pm 0.28$	$508 \pm 0.42$	$392 \pm 0.21$	$4.08 \pm 0.23$	$0.79 \pm 0.12$	$0.79 \pm 0.24$	-
Tangency points	45	$8075 \pm 0.81$	$8063 \pm 0.76$	$500 \pm 0.64$	$368 \pm 0.35$	$3.91 \pm 0.42$	$1.32 \pm 0.03$	$0.26 \pm 0.04$	$2.87 \pm 0.13$

**Table 1** Results of self-calibration by using either dot centres or points computed from bitangents as feature points.

are computed. The values obtained for the intrinsic parameters at  $0^{\circ}$  are quiet identical when using the dot centres or the points computed from bitangents. The residual error is of the order of 0.01 pixel. At  $30^{\circ}$ , the parameters are recovered when using bitangents but, as one could expect (see section 3.2), calibration failed when using dot centres. In Scheimpflug condition with a higher value of  $\alpha = 45^{\circ}$ , the use of bitangents allows accurate estimates: for example, the estimate of the Scheimpflug tilt (theoretical value:  $2.86^{\circ}$ ) is  $\theta = 2.87^{\circ} \pm 0.13^{\circ}$ . One can notice a relative deviation (inferior to 1%) of image distance  $p_x$  with respect to focal length  $f_x = 8000$ . This corresponds to the physical separation of the lens from the CCD device when Scheimpflug tilting.

## 6 CONCLUSION

Self-calibration of Scheimpflug cameras allows easy calibration by viewing a (planar) target at different locations in the depth of field. A bundle adjustment technique provides camera calibration together with target reconstruction provided that about a fifteen feature points is detected at a subpixel precision. We have demonstrated that the detection of dot centres induces an offset. In SPIV conditions, to neglect this offset implies to use small calibration dots with a radius inferior to 1 mm. We have proposed to reduce the calibration pattern to a set of two oriented coplanar ellipses having a larger size (20-30 mm) and to

take advantage of the invariance property of tangency points under perspective projection. 13 feature points can be computed from the four bitangents: tangency points and intersections between bitangents. Our detection method is based on a multi-scale edge detection at pixel precision and an ellipse fit. It provides a subpixel detection compatible with self-calibration requirements when few hundreds contour points are detected. Such a procedure tested in real conditions leads to a calibration pattern which is easy printable and usable for a large range of magnification.

### REFERENCES

- [1] Hinsch K D, Hinrichs H, Roshop A and Dreesen F 1993 Holographic and stereoscopic advance in 3D PIV. Holographic Particle Image Velocimetry *Proc. of Fluids Engineering Division, American Society of mechanical Engineers* vol 148, ed E P Rood (Washington, DC:ASME) p 33-6
- [2] Prasad A K and Jens K 1995 Scheimpflug stereocamera for particle image velocimetry in liquid flow *Appl. Opt.* **34** 7092-9
- [3] Soloff S, Adrian R and Liu Z C 1997 Distortion Compensation for generalised stereoscopic particle image velocimetry *Meas. Sci. Technol.* **8** 1441-54
- [4] Fournel T, Lavest J M, Coudert S and Collange F 2003 Self-calibration of PIV video-cameras in Scheimpflug condition (Espagne: Springer)
- [5] Lavest JM, Viala M and Dhome M 1998 Do we really need an accurate calibration pattern to acheive a reliable camera calibration *Proc. of ECCV98* (Freiburg: Germany) p 158-174
- [6] Tarel JP and Gagalowicz A 1995 Ellipse-based camera calibration *Traitement du Signal***12:2** p 177-187
- [7] Heikkila J 2000 Geometric camera calibration using circular control points *Pattern Analysis and Machine Intelligence IEEE Transactions***22(10)** p 1066 - 1077
- [8] Habert L 2005 Computing bitangents for ellipses *Proc. 17th Canadian Conference on Computational Geometry (CCCG'05)* p 294-297
- [9] A Fitzgibbon, M Pilu, and R B Fisher, Direct Least Square Fitting of Ellipses, In *IEEE Trans. Pattern Analysis and Machine Intelligence*, 21(5), pp. 476-480, 1999.
- [10] Triggs W, McLauchlan P, Hartly R and Fitzgibbon 2000 Bundle adjustment: a modern synthesis (Verlag: springer)
- [11] C Ducottet, T Fournel and C Barat, Scale-adaptive detection and local characterization of edges based on wavelet transform, In *Signal Processing*, 84: 2115-2137, 2004.